Journal of Applied Polymer Science

Enhanced Gas Separation Properties of Metal Organic Frameworks/ Polyetherimide Mixed Matrix Membranes

Cuijia Duan,[1,2] Guodong Kang,[1] Dandan Liu,[1] Lina Wang,[1] Can Jiang,[1,2] Yiming Cao,[1] Quan Yuan[1]

[1]Chinese Academy of Sciences, Dalian Institute of Chemical Physics, Dalian 116023, China

[2]University of Chinese Academy of Sciences, Beijing 100049, China

Correspondence to: Y. M. Cao (E-mail: ymcao@dicp.ac.cn)

ABSTRACT: Metal organic frameworks (MOFs) are supposed to be ideal additives for mixed matrix membranes (MMMs). In this article one kind of MOFs, $Cu_3(BTC)_2$, is synthesized, then directly incorporated into a model polymer (Ultem®1000) using N,N-dimethylacetamide as solvent. $Cu_3(BTC)_2$ particles are uniformly dispersed and there are no interfacial defects in the prepared MMMs when $Cu_3(BTC)_2$ loading is not more than 35 wt %, seen in SEM images. Pure gas permeation tests show that gas permeability increases obviously with $Cu_3(BTC)_2$ loading increase, while ideal selectivities of CO_2/N_2 and CO_2/CH_4 are almost unchanged. For MMM with the best separation property, CO_2 permeability increases about 2.6 times and CO_2/N_2 selectivity remains almost unchanged. Results about gas diffusivity and solubility indicate that gas diffusivity and solubility make contribution to gas permeability increase at the same time but in different ways. Gas permeation properties of MMMs are well predicted by Maxwell or Bruggeman model. © 2014 Wiley Periodicals, Inc. J. Appl. Polym. Sci. **2014**, *131*, 40719.

KEYWORDS: membranes; non-polymeric materials and composites; oil and gas; properties and characterization; separation techniques

Received 26 December 2013; accepted 10 March 2014

DOI: 10.1002/app.40719

INTRODUCTION

Membrane separation technology has shown great application potential in gas separation field such as air separation, hydrogen and heavy hydrocarbon recovery, CO_2 removal, and so on.[1] At present, organic polymers are the dominant materials for commercially available gas separation membranes.[2,3] However, their performances are always restricted by the so-called Robeson upper bound that generally comes from inevitable trade-off between permeability and selectivity. As a result, the inorganic membranes such as zeolite, carbon, and silica membranes are receiving more attentions in recent years owing to their excellent gas separation properties.[4] However, some drawbacks have inhibited their industrial application, such as tough defect-free structure control, material fragility and low packing density. Consequently, the concept of mixed matrix membranes (MMMs) was proposed, and related researches started from the 1970s by adding 5A zeolite into polydimethylsiloxane (PDMS) to form a heterogeneous membrane.[5] They can combine the advantages of organic and inorganic membranes, thus they are expected to own easy operation capability as well as satisfactory gas separation property.[6]

The inorganic particles, which are used as the additives for MMMs, can be commonly classified into two types: porous particles [such as molecular sieve,[7,8] activated carbon, and carbon nano-tubes (CNTs)[9]] and nonporous particles (like nano-scale TiO_2 and SiO_2).[10] Unfortunately, due to huge physical property difference between inorganic additives and organic polymer, it would be quite difficult to fabricate a well-dispersed and defect-free MMMs.[11] Particle aggregation and interfacial defects (large gaps between dispersed phase and continuous phase, the size of gaps is much bigger than gas molecule size) are the two major problems that would reduce gas selectivity of the prepared MMMs.[12] In order to mitigate their negative influences, the main efforts researchers are making include introducing functional groups onto polymer chain and modifying the inorganic particles. The later is more commonly used while it often causes gas permeability decrease. Recently, a new type of synthetic porous materials known as metal organic frameworks (MOFs) or porous coordination polymers (PCPs)[13] have been developed for MMM fabrication.

MOFs have large surface areas, tunable pore sizes, and strong adsorption capability for special gases such as CO_2. What's more, MOFs are inorganic–organic hybrid materials composed of metals and organic ligands which could modify the compatibility between MOF particles and polymer matrix, thus they are expected to be ideal additives for MMMs.[14] Some reports have revealed that even using unmodified MOFs as additives directly,

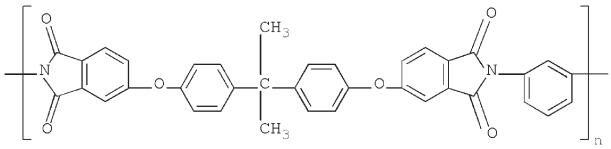

Figure 1. Chemical structure of Ultem®1000.

gas separation properties of the prepared MMMs still were obviously improved since the non-selective interfacial defects have been suppressed greatly. For example, by introducing MOF-5[15] and Cu-4,4′-bipyridine hexafluoro-silicate[16] into Matrimid®5218, improved gas permeabilities were achieved with CO_2/CH_4 selectivity remained unchanged.

Selecting proper combination of dispersed particles and polymers matrix is a key factor for high-property MMM preparation. $Cu_3(BTC)_2$ (also named as HKTUS-1[17,18]), as one kind of MOFs, has large BET area (1482 $cm^2\ g^{-1}$), good thermal stability (thermal decomposition temperature > 300°C), and high gas adsorption capacity (means good gas permeation property),[19–21] so it is supposed to be an ideal additive to prepare MMMs and improve their gas separation properties. Ultem®1000, a commercially available polyetherimide with low price, has good mechanical strength, excellent thermal and chemical stability. When serving as membrane material, Ultem®1000 shows excellent gas selectivity, however, its gas permeability is a little low. Thus, in this study $Cu_3(BTC)_2$ was directly added into Ultem®1000 to prepare $Cu_3(BTC)_2$/Ultem®1000 MMMs (C/U MMMs) and improve its gas permeability. Besides dispersed particles and polymer matrix, solvent is another important factor for high-property (defect-free) MMM fabrication.[22] To prevent interfacial defects in MMMs, non-polar solvents such as CH_2Cl_2, chloroform and benzene, which are not suitable to fabricate asymmetric membranes, were employed in most MMM preparations. In this article, N,N-dimethylacetamide (DMAc) commonly applied in commercial asymmetric membrane fabrication was used as solvent to fabricate defect-free C/U MMMs. Pure gas permeation tests were applied to investigate the gas permeability enhancements of C/U MMMs. What is more, detailed analyses had been made regarding gas permeability enhancement mechanism in terms of gas solubility and diffusivity in C/U MMMs. This article provided some information about the intrinsic gas separation properties of C/U MMMs, which will be necessary for hollow fiber membranes fabrication in our continued efforts.

EXPERIMENTAL

Materials and Reagents

1,3,5-benzenetricarboxylic acid (H_3BTC, AR) was obtained from Aladdin Industrial Inc. $Cu(NO_3)_2{\cdot}3H_2O$, methanol, ethanol, N,N-dimethylformamide (DMF), and N,N-dimethylacetamide (DMAc) were purchased from Liaodong Chemical Reagent Company, China. Ultem®1000 polymer (Figure 1) was obtained from GE Plastics and used as polymer matrix. H_3BTC, $Cu(NO_3)_2{\cdot}3H_2O$, ethanol, and DMF were used to synthesize $Cu_3(BTC)_2$ (Figure 2) without any further purification. Methanol and ID water were used to wash the synthesized $Cu_3(BTC)_2$. DMAc was dehydrated by mixing with activated 4A molecular sieve for at least 2 days before used for membrane fabrication, the weight ratio of molecular sieve to DMAc was in the range of 1/4 to 1/3. Gases for permeation tests are N_2, O_2, CH_4, and CO_2 with purity of at least 99.9%.

Synthesis of $Cu_3(BTC)_2$

$Cu_3(BTC)_2$ was synthesized by a modification process described by Liu et al.[19] Certain amount of H_3BTC was dissolved in the mixed solution of DMF and ethanol, and at the same time $Cu(NO_3)_2{\cdot}3H_2O$ was dissolved in DI water with certain concentration. Then $Cu(NO_3)_2$ aqueous solution was added into the H_3BTC/DMF/ethanol mixed solution slowly. The obtained solution was stirred at room temperature for 10 minutes, and then poured into a Teflon lined steel autoclave (100 ml) and heated at 85°C for 8 h. $Cu_3(BTC)_2$ crystal was obtained by filtration, then it was washed with the mixture of ethanol/DI water and methanol in sequence, and finally dried at 110°C for 24 h.

Preparation of Membranes

Both $Cu_3(BTC)_2$ and Ultem®1000 polymer were dehydrated at 110°C for 24 h before membrane fabrication. The $Cu_3(BTC)_2$ powder was dispersed into DMAc with mechanical agitation. Ultem®1000 polymer was dissolved in DMAc to form a homogeneous solution. A "priming" technique was used to make the $Cu_3(BTC)_2$ particles more compatible with the Ultem®1000 polymer matrix and prevent interfacial defects. First, 10 wt% of the total polymer solution was added into the $Cu_3(BTC)_2$ solution accompanying with mechanical agitation, then the residual polymer was added in batches. When the polymer was completely added, further agitation and sonication were applied to ensure the $Cu_3(BTC)_2$ mix well with the polymer. The $Cu_3(BTC)_2$/Ultem®1000 mixed solution was cast onto a clean glass substrate and heated to evaporate the solvent. The formed membranes were peeled off from the glass and further dried in vacuum oven. The pure polymer membrane was fabricated in the same process.

In this article, in most cases prepared $Cu_3(BTC)_2$/Ultem®1000 MMMs will be expressed as C/U-X in which C and U represent

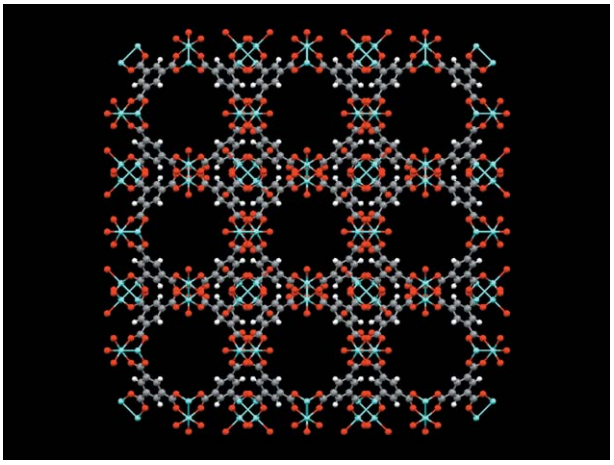

Figure 2. Chemical structure of $Cu_3(BTC)_2$ (Cu, blue; C, gray; O, red; H, white).[17] [Color figure can be viewed in the online issue, which is available at wileyonlinelibrary.com.]

$Cu_3(BTC)_2$ and Ultem®1000 polymer respectively; X means how much $Cu_3(BTC)_2$ is in $Cu_3(BTC)_2$/Ultem®1000 MMMs in unit of weight percentage, in other words, $Cu_3(BTC)_2$ loading. By adjusting the amount of $Cu_3(BTC)_2$ added, C/U MMMs with different $Cu_3(BTC)_2$ loadings were obtained, and the loading was determined by eq. (1)

$$Cu_3(BTC)_2 \text{ loading(wt \%)} = \left[\frac{\text{wt.}Cu_3(BTC)_2}{\text{wt.}Cu_3(BTC)_2 + \text{wt.Ultem}}\right] \times 100 \text{ (wt \%)} \quad (1)$$

Characterization

The nitrogen sorption–desorption isotherm of $Cu_3(BTC)_2$ was recorded using Autosorb IQ analyzer at liquid nitrogen (77K) to calculate its BET surface area and total pore volume. Before testing, sample was degassed under vacuum at 180°C for 18 h.

Thermal stabilities of $Cu_3(BTC)_2$ and prepared membranes were analyzed by Thermo-gravimetric analysis (TGA) using STA449F3 in the range of 25–800°C at a heat ratio of 10°C min^{-1} under N_2 protection.

Power X-ray diffraction (XRD) of samples was carried out with a D/Max2500 VB/PC spectrometer using Cu Kα radiation in the range of 3–50° at a step of 5° min^{-1} (40 kV, 200 mA) to analyze the structure of $Cu_3(BTC)_2$ particles and membranes.

The chemical structures of $Cu_3(BTC)_2$ and membranes were determined by a Nicolet iS5 Fourier transform infrared spectroscopy (FTIR) spectrophotometer equipped with a single-bounce attenuated total reflectance (ATR) accessory.

The cross-section scanning electron microscopy (SEM) images of the C/U MMMs with different loadings were examined using JSM6360-LV (20Kv). Before testing, the C/U MMMs were frozen in liquid nitrogen, and broken off quickly. The cross sections of MMMs were coated with gold using a sputtering system.

Gas Permeation Test

Gas permeation properties of membranes were tested by homemade gas permeameter using variable-pressure constant-volume method. First, membrane was set in a permeation cell, and the whole test system was degasses at 35°C. Then, tested gas was introduced on the upstream side, and the permanent pressure on the downstream side was monitored using a MKS-Baratron pressure transducer. When gas permeation reached steady state, permeability (P) of O_2, N_2, CH_4, and CO_2 were calculated by eq. (2)

$$P = \frac{22414}{A} \times \frac{V}{RT} \times \frac{L}{p} \times \frac{dp}{dt} \quad (2)$$

where, A is the membrane area (cm^2), L is the membrane thickness (cm), p is the upstream pressure (cmHg), V is the downstream volume (cm^3), R is the universal gas constant [6236.56 cm^3(STP) cmHg mol^{-1} K^{-1}], T is the absolute temperature (K), and dp/dt is the permeation rate (cmHg s^{-1}). All membranes were tested at 35°C and 3.5 atm.

For the heterogeneous membranes, several kinds of models have been developed to calculate their gas permeabilities, and Maxwell model is the most commonly used one. According to Maxwell model which proposes that the solid particles are homogeneously dispersed in the continuous polymer matrix, the effective gas permeability (P_{eff}) of the MMMs can be determined by eq. (3)

$$P_{eff} = P_c\left[\frac{P_d + 2P_c - 2\Phi_d(P_c - P_d)}{P_d + 2P_c + \Phi_d(P_c - P_d)}\right] \quad (3)$$

where P_c is the gas permeability in the continuous phase and P_d is the value for dispersed phase. Φ_d is the volume ratio of the dispersed phase. When $P_d >> P_c$, the Maxwell model can be abbreviated to eq. (4)

$$P_{eff} = P_c\left(\frac{1 + 2\Phi_d}{1 - \Phi_d}\right) \quad (4)$$

the Maxwell model assumes that the gas transport around dispersed particles are not affected by their neighbor particles, thus it is only applicable to MMMs which have low additive loading. In order to calculate the permeability of MMMs more accurately, Bruggeman et al.[23] developed a modified version of Maxwell model, which have considered the interactivity between the nearby particles. The effective permeability (P_{eff}) is determined by eq. (5)

$$\left[\frac{(P_{eff}/P_c) - (P_d/P_c)}{1 - (P_d/P_c)}\right]\left(\frac{P_{eff}}{P_c}\right)^{-1/3} = (1 - \Phi_d) \quad (5)$$

when $P_d >> P_c$, eq. (5) could be abbreviated to eq. (6)

$$\left(\frac{P_{eff}}{P_c}\right)^{-1/3} = (1 - \Phi_d) \quad (6)$$

the experimental data were compared with the gas permeabilities calculated from Maxwell and Bruggeman model to find out if the particles were as well dispersed in MMMs as models proposed.

The ideal selectivity ($\alpha_{i/j}$) of two different gases (i and j) was determined by eq. (7)

$$\alpha_{i/j} = P_i/P_j \quad (7)$$

the gas transport through a dense polymeric membrane is usually described by solution–diffusion mechanism. Time-lag method is commonly used to determine the pure gas diffusivity (D), as shown in eq. (8)

$$D = L^2/6\theta \quad (8)$$

where L is the membrane thickness (cm) and θ is lag time (s). Gas solubility (S) is calculated by diffusion-solution model (eq. (9)).

$$S = P/D \quad (9)$$

All data of gas permeabilities, diffusivities, and solubilities for membranes have been repeated and average values were finally applied. The relative error for all data was within acceptable range.

RESULTS AND DISCUSSION

Characterization

Surface Area of $Cu_3(BTC)_2$. Usually MOFs have outstanding gas adsorption properties owing to their large surface areas; that is why they could be used as additives to improve gas separation

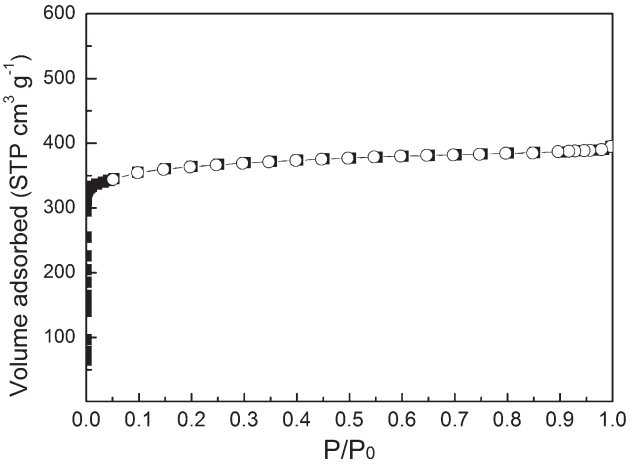

Figure 3. Nitrogen adsorption–desorption isotherm of $Cu_3(BTC)_2$.

properties of MMMs. In this section, BET analysis was applied to the prepared $Cu_3(BTC)_2$. As shown in Figure 3 it can be seen that nitrogen adsorption–desorption isotherm of $Cu_3(BTC)_2$ followed a typical type I isotherm which indicates the main partition of pores in the structure are in micro-level, and the result is consistent with the literatures[18,19,21,24] which reported the pore size of $Cu_3(BTC)_2$ was in the range of 0.35–0.9nm. The BET specific surface area and pore volume of the prepared $Cu_3(BTC)_2$ calculated from the isotherm were equal or even larger compared with the literatures (Table I). Thus, it can be deduced that the gas adsorption capacity of $Cu_3(BTC)_2$ in this article is comparable with the literature results which showed high adsorption properties for various gases.[21]

Thermal Stability of MOFs and Membranes

Additives in MMMs must possess sufficiently high thermal stability to prevent any possible decomposition during thermal treatment in membrane fabrication. TGA curve of $Cu_3(BTC)_2$ shown in Figure 4 illustrates that there were two periods during the weight loss: the first period (between 30 and 110°C) could be attributed to volatilization of residual solvents (methanol, ethanol or water), and the second period starting around 310°C was ascribed to the organic ligand decomposition in $Cu_3(BTC)_2$. 310°C was already much higher than what the heat treatment demands.

TGA curves of the pure Ultem®1000 membrane and C/U-20 MMM (as a representative of all MMMs) were also shown in Figure 4. Pure Ultem®1000 membrane expressed the best thermal stability with a decomposition temperature as high as

Table I. Structure Properties of $Cu_3(BTC)_2$ in this Article and the Literatures

BET surface area (m^2 g^{-1})	Pore volume (cm^3 g^{-1})	References
1439	0.612	This article
1071	0.496	Ref. (18)
1482	0.828	Ref. (19)
1555	0.710	Ref. (21)

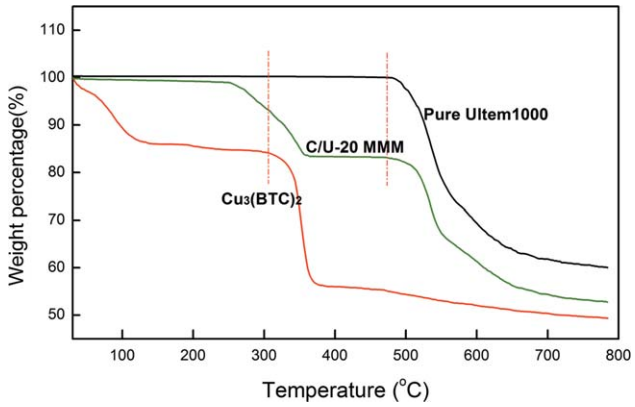

Figure 4. TGA curves of $Cu_3(BTC)_2$, pure Ultem®1000, and C/U-20 MMM (a representative of all MMMs). [Color figure can be viewed in the online issue, which is available at wileyonlinelibrary.com.]

495°C. Adding $Cu_3(BTC)_2$ into Ultem®1000 will obviously degrade its thermal stability. First, an extra weight loss around 250°C could be seen for C/U-20 MMM, which could be ascribed to the evaporation of adsorbed solvent in $Cu_3(BTC)_2$ such as DMAc or water; after 310°C a sharper weight loss curve could be seen, which was attributed to the $Cu_3(BTC)_2$ decomposition; at the end, the decomposition of Ultem®1000 in C/U MMMs happened around 500°C that was close to pure Ultem®1000 membrane.

$Cu_3(BTC)_2$ Structure Analysis by XRD. Figure 5(b) shows that the XRD pattern of our prepared $Cu_3(BTC)_2$ is consistent with the literatures,[20,25] thus it could be affirmed that our $Cu_3(BTC)_2$ also has similar ordered and crystalline structure. Besides $Cu_3(BTC)_2$, pure Ultem®1000 membrane and C/U-20 MMM (as a representative of all C/U MMMs) were also characterized by XRD. For Ultem®1000 polymer we did not see any obvious peaks in its XRD pattern [Figure 5(a)]. However, from the XRD pattern of the C/U-20 [Figure 5(c)] we can clearly see a combination of the crystalline peaks of $Cu_3(BTC)_2$ and waved curve

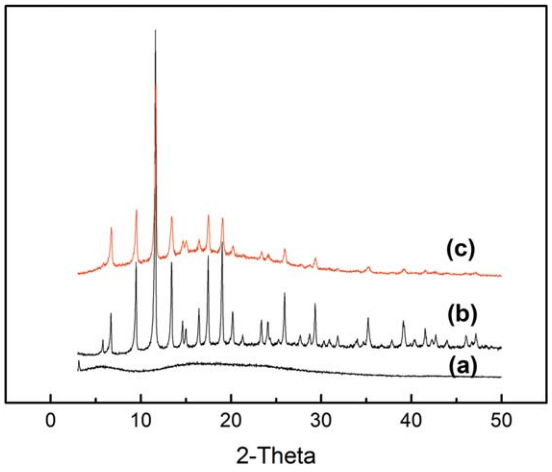

Figure 5. XRD patterns of (a) pure Ultem®1000 membrane, (b) $Cu_3(BTC)_2$, and (c) C/U-20 MMM (a representative of all C/U MMMs). [Color figure can be viewed in the online issue, which is available at wileyonlinelibrary.com.]

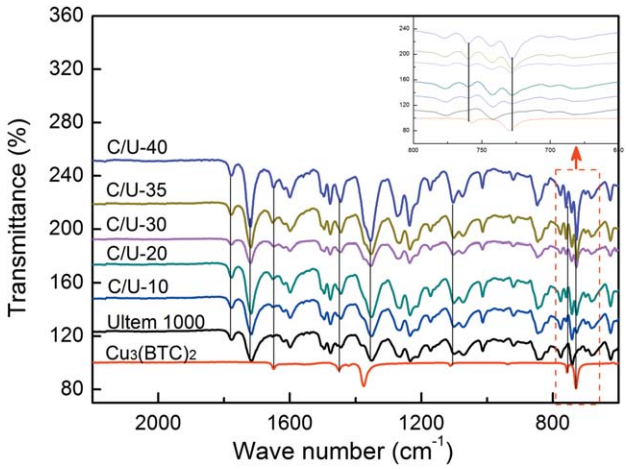

Figure 6. ATR-FTIR spectra of $Cu_3(BTC)_2$, pure Ultem®1000 membrane, and C/U MMMs with different loadings. [Color figure can be viewed in the online issue, which is available at wileyonlinelibrary.com.]

of pure Ultem®1000 membrane. Thus it can be concluded that $Cu_3(BTC)_2$ maintained its original structure integrity in the C/U MMMs, which has been confirmed by TGA test result.

Chemical Structure Analysis by ATR-FTIR. ATR-FTIR spectra of $Cu_3(BTC)_2$, pure Ultem®1000, and C/U MMMs with different loadings were shown in Figure 6. The adsorption bands at 728 cm^{-1} and 759 cm^{-1} in the ATR-FTIR spectra of $Cu_3(BTC)_2$ are attributed to C—H symmetric stretching vibration of H_3BTC, which can be regarded as the characteristic bands for $Cu_3(BTC)_2$. The weak band at 1111 cm^{-1} is attributed to C—O—Cu stretching vibration, and the bands at 1450 and 1649 cm^{-1} are due to C=C skeleton vibration of benzene. The adsorption bands at 1776 cm^{-1} (symmetric stretch of the carbonyl group), 1716 cm^{-1} (asymmetric stretch of the carbonyl group), and 1351 cm^{-1} (C—N stretch) are the characteristic bands of pure Ultem®1000 membrane. In the ATR-FTIR spectra of the C/U MMMs, the characteristic bands of $Cu_3(BTC)_2$ as well as Ultem®1000 membrane were found, that confirmed the existence of $Cu_3(BTC)_2$ in the C/U MMMs. As we expected, the characteristic bands of $Cu_3(BTC)_2$ (728 and 759 cm^{-1}) in the spectra of C/U MMMs became stronger as the $Cu_3(BTC)_2$ loading increased.

MMMs Morphology Examination by SEM. Existence of non-selective defects at the additive/polymer matrix interface is one of the main problems for MMMs fabrication since it will influence the gas separation property of MMMs directly. Besides proper additive and polymer matrix, solvent is another significant factor for defect-free MMM fabrication. To prevent interfacial defects, non-polar solvents such as benzene, toluene, CH_2Cl_2, and chloroform were most commonly used in former literature MMMs. However, these solvents are poisonous and volatile, and polymers have poor solubility in them, that are most likely killing the possibility of their industrial applications. In this article, profiting from the excellent compatibility between synthesized $Cu_3(BTC)_2$ and Ultem®1000, DMAc, a common polar solvent with high boiling point, was used to fabricate the C/U MMMs. The solubility of commercial polymers such as polysulfone (PSf), poly (ether sulfone) (PES), polyimide (PI), and polyetherimide (PEI) in DMAc are pretty good, thus DMAc has been widely applied in industry. To certain extent, this solvent selection means our MMMs could own better application potential.

Cross-section SEM images of the prepared C/U MMMs were taken to preliminary investigate their interfacial coalescence conditions. Figure 7(a–e), respectively show the cross-section of C/U-10, C/U-20, C/U-30, C/U-35, and C/U-40 with different magnifications. It can be seen that there were no obvious $Cu_3(BTC)_2$ aggregations, all $Cu_3(BTC)_2$ particles dispersed quite uniformly throughout the polymer matrix in all C/U MMMs.

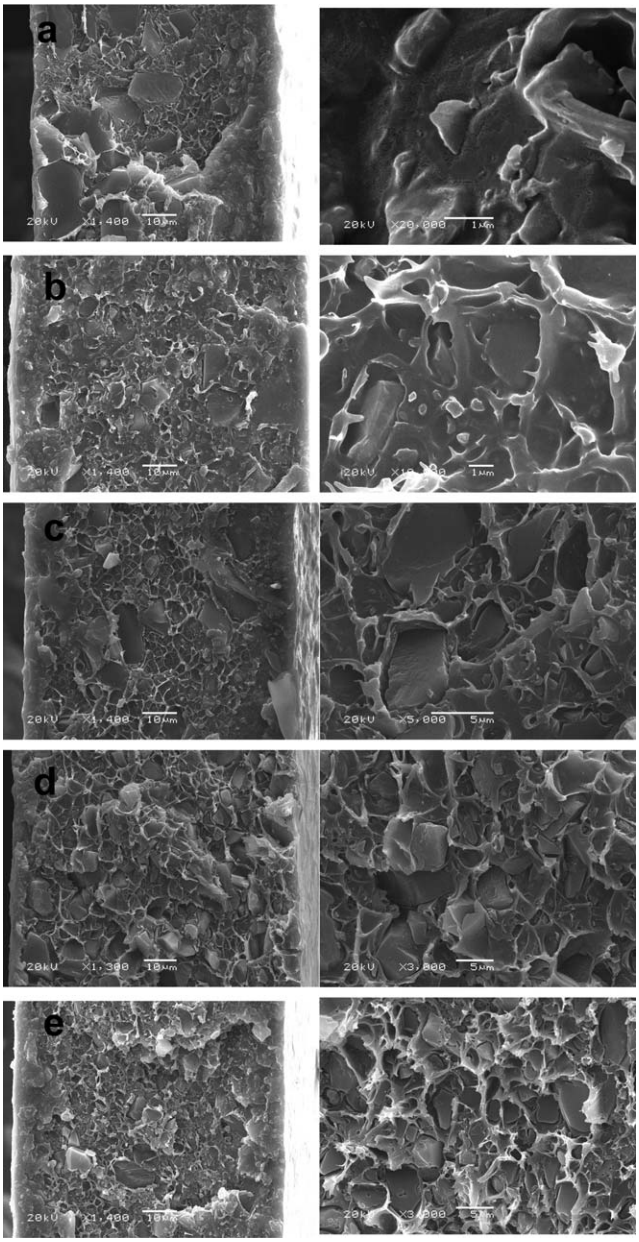

Figure 7. Cross-section SEM images of (a) C/U-10, (b) C/U-20, (c) C/U-30, (d) C/U-35, and (e) C/U-40.

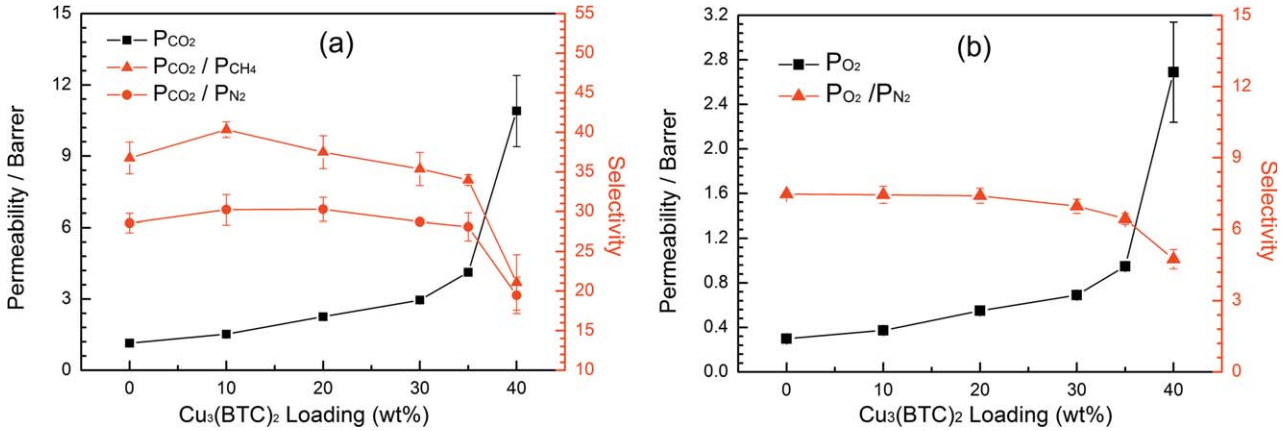

Figure 8. CO_2, O_2 permeability and ideal selectivity [(a) CO_2/N_2 and CO_2/CH_4, and (b) O_2/N_2] of pure Ultem®1000 membrane and C/U MMMs with different loadings at 35°C and 3.5 atm. [Color figure can be viewed in the online issue, which is available at wileyonlinelibrary.com.]

For C/U MMMs with lower $Cu_3(BTC)_2$ loadings (10 and 20 wt %), $Cu_3(BTC)_2$ particles were wetted quite well by the polymer. At 30 wt % loading, interfacial combination of $Cu_3(BTC)_2$ and polymer matrix became a little weaker, however, $Cu_3(BTC)_2$ still connected well with polymer. As the loading was as high as 35 wt %, quite slight interfacial gaps appeared but were still not obvious. There are two possible reasons to explain the phenomena: firstly, the polymer chain is very flexible that enables it wound around the particles easily; another could be the organic ligand and super large surface area of $Cu_3(BTC)_2$ that would enhance the compatibility between two phases and eliminate the interfacial defects greatly.[12,26] Continued attempt to increase $Cu_3(BTC)_2$ loading to 40 wt % [Figure 7(e)] seemed to generate some interfacial defects which would affected gas separation property of MMMs. As a conclusion, it can be initially confirmed that defect-free C/U MMMs were obtained within 0–35 wt % $Cu_3(BTC)_2$ loading.

Gas Permeation Property

Influence of $Cu_3(BTC)_2$. From all physical characterizations and SEM examination in former sections, we have already known that synthesized $Cu_3(BTC)_2$ can maintain its crystalline structure and chemical integrity during MMMs fabrication, and there were no obvious interfacial defects in the C/U MMMs with loading not more than 35 wt %. Next, gas separation properties of pure polymer membrane and C/U MMMs with different $Cu_3(BTC)_2$ loadings were tested to investigate the influences of $Cu_3(BTC)_2$ on the C/U MMMs.

From Figure 8(a) it can be seen that, within the range of 0–30 wt % loading, CO_2 permeability increased with $Cu_3(BTC)_2$ loading increase, at the same time CO_2/N_2 and CO_2/CH_4 selectivity were almost unchanged compared with pure Ultem®1000 membrane. As the loading up to 35 wt %, a sharper permeability increase was achieved, at this point CO_2 permeability reached up to 4.13 Barrer that was 2.62 times higher if compared with pure Ultem®1000 membrane; on the other hand, the selectivity of CO_2/N_2 and CO_2/CH_4 showed slight decrease but were still in the same level with pure polymer membrane. However, when $Cu_3(BTC)_2$ loading was up to 40 wt % gas permeability substantially increased but accompanying obvious decrease of CO_2/N_2 and CO_2/CH_4 selectivity. Similar tendency could be seen from Figure 8(b) in term of O_2 permeability and O_2/N_2 selectivity.

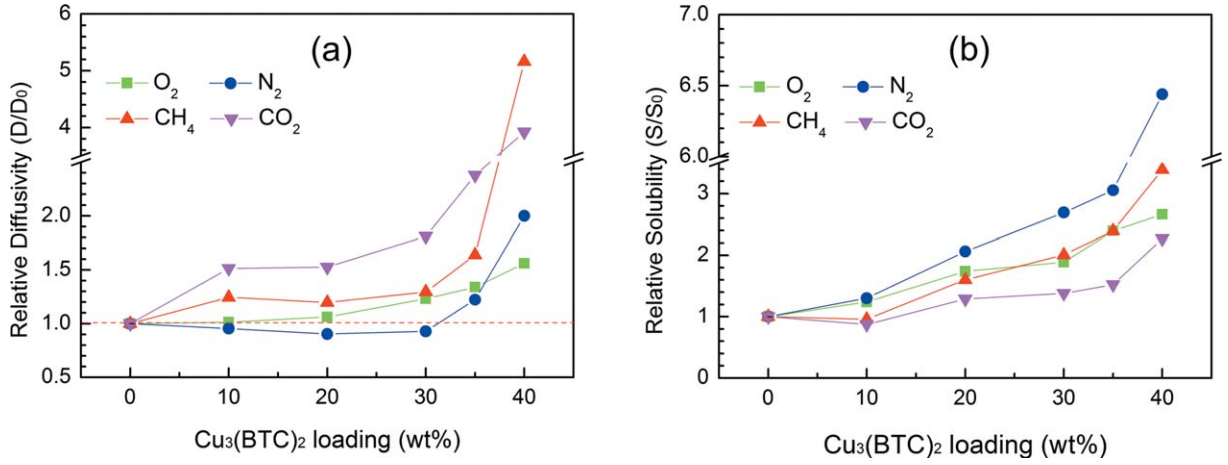

Figure 9. Relative gas diffusivities and solubilities of pure Ultem®1000 membrane and C/U MMMs with different loadings. [Color figure can be viewed in the online issue, which is available at wileyonlinelibrary.com.]

Table II. Physical Parameters of Gas Molecules Tested in this Article

Gas molecule	Kinetic diameter/Å	Adsorption in $Cu_3(BTC)_2$/[cm^3(STP)]/(cm^{-3} cmHg)[a]	Solubility in Ultem® 1000/[cm^3(STP)]/(cm^{-3} cmHg)[b]
O_2	3.46	-	0.00489
N_2	3.64	0.0585	0.00357
CH_4	3.76	0.158	0.0168
CO_2	3.3	0.596	0.0647

[a] Gas adsorption was tested at 35°C and 3.5 atm.[21]
[b] Gas solubility was tested at 35°C and 3.5 atm, in this article.

For gas permeability enhancement within 0–35 wt % loading, there could be two main reasons: first reason is the high gas permeation properties of the added particles profiting from their micro-porous structures; second may be the quite slight interfacial gaps between the particles and polymer matrix, which could permit gas pass through but have little effect on gas selectivity. According to the results in Figure 8, it seems that, for MMMs with the lower loadings ($\leq$ 30 wt %), the first reason should be the main cause for their gas permeability increases. Added $Cu_3(BTC)_2$ could greatly reduce gas permeation resistance of MMMs, thus their gas permeabilities showed obvious increases and gas selectivities remained almost unchanged; at the same time not too large $Cu_3(BTC)_2$ loading will not generate interfacial gaps, that could be confirmed by their SEM images in Figure 7(a–c). Further loading increase would enlarge the possibility of slight interfacial gap formation, which could well explain the much sharper gas permeability increase and slight selectivity decrease of C/U MMM with 35 wt %. It should be pointed out that "slight interfacial gaps" have intrinsic difference with commonly called "interfacial defects" which would substantially reduce gas selectivity of MMMs, while gas selectivity of C/U-35 was just little degraded and still in the same level with pure Ultem®1000 membrane. As $Cu_3(BTC)_2$ loading up to 40 wt % "slight interfacial gaps" grew to "interfacial defects" [seen in Figure 7(e)], that should be the main cause for substantial permeability increase and obvious selectivity decrease.

Further Analysis Through Diffusivity and Solubility. Gas permeation in dense polymeric membranes is usually described by widely accepted "solution–diffusion" mechanism. For gas permeation in pure MOF membranes, it follows "absorption–diffusion" mechanism which is very similar to "solution–diffusion" mechanism. The gas separation properties of MOF membranes are partially determined by their gas adsorption capacity which is almost same as gas solubility in the polymeric membranes. Thus, we believe "solution–diffusion" mechanism could also be applied to investigate the gas permeation properties of the mixed-matrix membranes.

In former literatures, gas diffusivities of MMMs changed in different ways as porous particles were added, because gas diffused through polymer matrix and porous additives at the same time, the pore size, shape, and flexibility of additives had great effect on gas diffusivity.[15,16,27] As we already know, MOF is one kind of micro-porous materials with super high surface area and pore volume, thus we believe gas diffusivities of MMMs would be substantially influenced by MOFs. In this section, the relative gas diffusivities based on pure Ultem®1000 membrane for all prepared C/U MMMs were presented in Figure 9(a) to study the influence of $Cu_3(BTC)_2$ on gas diffusion process.

From Figure 9(a) it can be clearly seen that, except N_2 which only showed increased gas diffusivity when the loading was higher than 30 wt %, diffusivities of all other tested gases including CO_2, CH_4, and O_2 increased within all measured loadings, and a relatively sharper increase could be seen after 35 wt % loading, especially for MMMs with 40 wt % loading CO_2 and CH_4 diffusivity of which exhibited substantial increases. Interestingly their diffusivity increase tendencies were almost consistent with their absorption capabilities in $Cu_3(BTC)_2$ particles as listed in Table II. This sounds reasonable since their diffusivity increases were specifically caused by added $Cu_3(BTC)_2$ particles.

Unfortunately it is difficult to determine the cause of the decreased N_2 diffusivity of C/U MMMs with lower loadings ($\leq$30 wt %), poor adsorption capacity and large molecule size (3.64 Å) of N_2 may be the reasons. However, in a certain extent, this phenomenon could prove that when the $Cu_3(BTC)_2$ loading is not more than 30 wt % there were almost no interfacial gaps in MMMs which would permit gas to pass through and bring

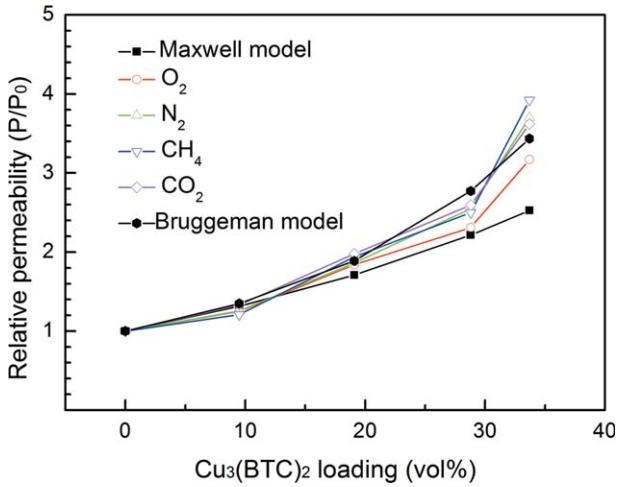

Figure 10. Relative gas permeabilities of pure Ultem®1000 membrane and C/U MMMs with different loadings (vol %) in this article compared with Maxwell and Bruggeman model. [Color figure can be viewed in the online issue, which is available at wileyonlinelibrary.com.]

Table III. The Mixed Matrix Membranes in the Literatures and this Article with Ultem®1000 as Polymer Matrix

Membrane	P_{CO2}	P_{CO2}/P_{CH4}	Solvent	References
Pure Ultem	1.14	36.77	DMAc	This article
$Cu_3(BTC)_2$/Ultem	4.13	33.99		
Pure Ultem	1.95	30.3	-	Ref (26)
IRMOF-1/Ultem	2.97	26.3		
Pure Ultem	1.2	38	DCM	Ref (29)
ZIF-90/Ultem	2.9	39		
Pure Ultem	0.63	79.6	Toluene	Ref (30)
HNT/Ultem	1.19	47.76		

about gas diffusivity increase. More obvious diffusivity increases for all tested gases when $Cu_3(BTC)_2$ loading increased to higher value of 35 wt % possibly revealed the formation of slight interfacial gaps, and substantial diffusivity increase at 40 wt % indicated the appearance of interfacial defects in MMMs. These above conclusions were consistent with our analysis from SEM images of C/U MMMs with different loadings.

As we mentioned earlier, gas permeation through MMMs follows the "solution–diffusion" mechanism, thus it is also necessary to find out what is the relationship between gas solubility and $Cu_3(BTC)_2$ loading. Similar to gas diffusivities, the relative gas solubilities of prepared membranes were presented in Figure 9(b). Solubilities for all gases increased obviously with $Cu_3(BTC)_2$ loading increase, and this could be possibly explained by high gas absorption capability of $Cu_3(BTC)_2$ (Table II) which owns extremely micro-porous structure. What should be mentioned here is that although all gas solubility increased with $Cu_3(BTC)_2$ loading, the increase order was $N_2>O_2>CH_4>CO_2$. Intrinsic gas solution selectivities of Ultem®1000 for CO_2/CH_4, CO_2/N_2, and CH_4/N_2 are higher than prepared $Cu_3(BTC)_2$ particles (shown in Table II), so adding $Cu_3(BTC)_2$ into Ultem®1000 would reduce the total apparent gas solution selectivity of C/U MMMs. The selectivity decrease may explains the phenomenon that larger relative solubility increases were seen for gases with original lower solubilities.

So based on results in Figure 9 and additional analysis, it could be concluded that CO_2 diffusivity increase made more contribution to its permeability increase, and for N_2 its permeability increase seemed to mainly profit from its solubility increase. Compared with them, permeability increases of O_2 and CH_4 were more likely a joint effort of diffusivity and solubility increase.

MMMs Performance

Comparison with Models. Maxwell and Bruggeman Model are the most commonly used methods to predict the gas permeability of MMMs, and the abbreviated Maxwell and Bruggeman Model (eqs. (4) and (6)) were applied in this study since the gas permeabilities of pure Ultem®1000 membrane (in the range of 0.01–1 Barrer) is far lower than that of $Cu_3(BTC)_2$ membrane (100–10000 Barrer).[28] The relative gas permeabilities of membranes were calculated through dividing the permeabilities of membranes by that of pure Ultem®1000 membrane, and they were compared with Maxwell and Bruggeman model to further investigate the properties of C/U MMMs. Gas permeability of C/U-40 was excluded because of the existence of obvious interfacial defects. From Figure 10 it can be seen that, with lower $Cu_3(BTC)_2$ loading, our experimental data were

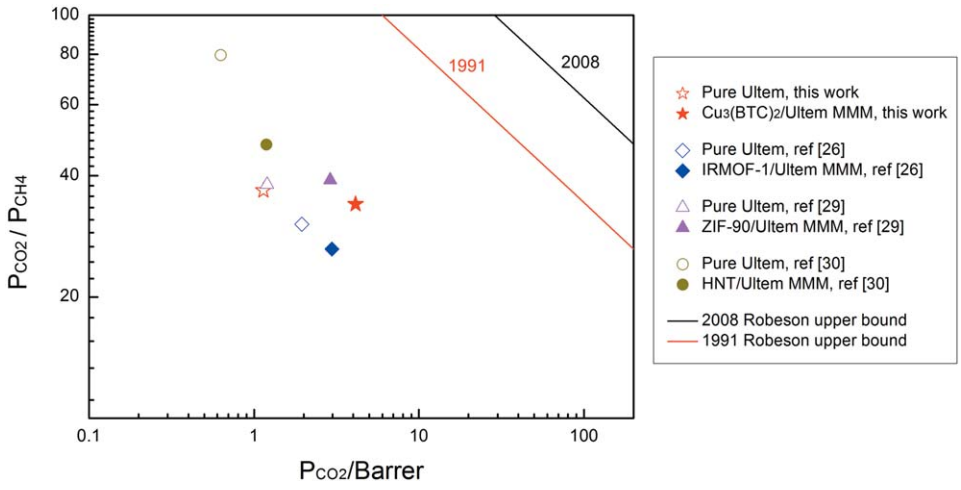

Figure 11. Performance of dense MMMs using Ultem®1000 as polymer matrix and different particles as dispersed phase with respect to Robeson upper bound curves. [Color figure can be viewed in the online issue, which is available at wileyonlinelibrary.com.]

quite close to the predicted values of both models. When the loading was increased to 30 wt % and higher, the experimental data were obviously closer to the value from Bruggeman model, this could be easily explained since the Bruggeman model has considered the influence of nearby particles on the gas permeation through MMMs. At 35 wt % loading, gas permeability even exceeded the predicted value of Bruggeman model, that could be owing to the existence of slight interfacial gaps between $Cu_3(BTC)_2$ and polymer matrix which had been proved in former Sections. Though there were a few deviations, the gas permeabilities of C/U MMMs with different $Cu_3(BTC)_2$ loadings were well predicated by the Maxwell or Bruggeman model. Thus, it can be deemed that the C/U MMMs in this article were close to the hypothesized ideal states of Maxwell and Bruggeman Model.

Compared with the Literature Results. First, as we have mentioned earlier, compared with the MMMs in literatures (shown in Table III), one possible advantage of our MMMs could be the solvent we used, DMAc, which has high boiling point and good solubility for polymers and is widely applied in industrial membrane fabrication, that could greatly widen the practical application possibility of C/U MMMs in this article.

Second, the gas separation property of C/U MMMs was compared with the literature[26,29,30] which also chose Ultem®1000 as polymer matrix while different porous particles as additives (shown in Table III). It can be seen that our C/U MMM with a $Cu_3(BTC)_2$ loading of 35 wt % showed the highest CO_2 permeability of 4.13 Barrer and comparable selectivity of CO_2/CH_4. Though, in term of CO_2/CH_4 selectivity, HNT/Ultem was an exception since its value was 47.76 which was higher than 33.99 from our work, unfortunately its CO_2 permeability was sadly as low as 1.19 Barrer. Since the intrinsic gas separation property of Ultem®1000 which is a model polymer with low price and excellent physical property are not high, the gas separation properties of MMMs with Ultem®1000 as polymer matrix are hard to exceed Robeson upper bound. However, it can be seen from Figure 11 that, as $Cu_3(BTC)_2$ added, gas separation property of membranes were obviously improved compared with pure polymer membrane and were closing to Robeson Upper bound. So we believe that C/U MMMs prepared in this article can perform a better gas separation property and have great potential for later commercial application.

CONCLUSIONS

$Cu_3(BTC)_2$ was synthesized and mixed with Ultem®1000 to fabricate C/U MMMs with different loadings. Characterization results (TGA, XRD, and ATR-FTIR) proved that $Cu_3(BTC)_2$ had maintained its structural integrity in the prepared C/U MMMs. From the SEM images of C/U MMMs it could be preliminarily determined that there were no obvious interfacial defects between $Cu_3(BTC)_2$ and Ultem®1000 polymer matrix when $Cu_3(BTC)_2$ loading was not more than 35 wt %. This was further proved by the gas separation properties of C/U MMMs: gas permeabilities increased substantially with $Cu_3(BTC)_2$ loading increase meanwhile their ideal gas selectivities were almost unchanged compared with pure Ultem®1000 membrane. Continued analysis based on gas diffusivities and solubilities in MMMs revealed that CO_2 permeability enhancement was mainly attributed to its diffusivity increase while N_2 seemed to profit from its solubility increase. Calculation results showed that gas permeabilities of the C/U MMMs in this article were well predicted by Maxwell or Bruggeman model. At the end a comparison was made between MMMs in this article and literature reported MMMs which used same Ultem®1000 as polymer matrix and different porous particles as additives. From the comparison results it can be clearly concluded that our prepared C/U MMMs performed much better gas separation properties.

ACKNOWLEDGMENTS

We gratefully acknowledge the financial support from National High Technology Research and Development Program of China (2012AA03A611).

REFERENCES

1. Chen, X. Y.; Kaliaguine, S. *J. Appl. Polym. Sci.* **2013**, *128*, 380.
2. Scholes, C. A.; Stevens, G. W.; Kentish, S. E. *Fuel* **2012**, *96*, 15.
3. Shen, Y.; Lua, A. C. *J. Appl. Polym. Sci.* **2010**, *116*, 2906.
4. Rao, A. P.; Desai, N. V.; Rangarajan, R. *J. Scientif. Indust. Res.* **1997**, *56*, 518.
5. Nik, O. G.; Chen, X. Y.; Kaliaguine, S. *J. Memb. Sci.* **2012**, *413*, 48.
6. Aroon, M. A.; Ismail, A. F.; Matsuura, T.; Montazer-Rahmati, M. M. *Sep. Purific. Technol.* **2010**, *75*, 229.
7. Kanehashi, S.; Gu, H.; Shindo, R.; Sato, S.; Miyakoshi, T.; Nagai, K. *J. Appl. Polym. Sci.* **2013**, *128*, 3814.
8. Huang, Z.; Li, Y.; Wen, R.; Teoh, M. M.; Kulprathipanja, S. *J. Appl. Polym. Sci.* **2006**, *101*, 3800.
9. Ismail, A. F.; Goh, P. S.; Sanip, S. M.; Aziz, M. *Sep. Purific. Technol.* **2009**, *70*, 12.
10. Suzuki, T.; Yamada, Y. *J. Appl. Polym. Sci.* **2013**, *127*, 316.
11. Mahajan, R.; Burns, R.; Schaeffer, M.; Koros, W. J. *J. Appl. Polym. Sci.* **2002**, *86*, 881.
12. Chung, T.-S.; Jiang, L. Y., Li, Y.; Kulprathipanja, S. *Prog. Polym. Sci.* **2007**, *32*, 483.
13. Li, J.-R.; Kuppler, R. J.; Zhou, H.-C. *Chem. Soc. Rev.* **2009**, *38*, 1477.
14. Zornoza, B.; Tellez, C.; Coronas, J.; Gascon, J.; Kapteijn, F. *Microp. Mesop. Mater.* **2013**, *166*, 67.
15. Perez, E. V.; Balkus Jr, K. J.; Ferraris, J. P.; Musselman, I. H. *J. Memb. Sci.* **2009**, *328*, 165.
16. Zhang, Y.; Musselman, I. H.; Ferraris, J. P.; Balkus Jr, K. J. *J. Memb. Sci.* **2008**, *313*, 170.
17. Chui, S. S. Y.; Lo, S. M. F.; Charmant, J. P. H.; Orpen, A. G.; Williams, I. D. *Science* **1999**, *283*, 1148.
18. Basu, S.; Cano-Odena, A.; Vankelecom, I. F. J. *J. Memb. Sci.* **2010**, *362*, 478.
19. Jinchen Liu, J. T. C. *J. Phys. Chem. C* **2007**, *111*, 9305.
20. Zhijian Liang, M. M. *Energy Fuels* **2009**, *23*, 2785.

21. Moellmer, J.; Moeller, A.; Dreisbach, F.; Glaeser, R.; Staudt, R. *Microp. Mesop. Mater.* **2011**, *138*, 140.
22. Rajiv Mahajan, W. J. K. *Ind. Eng. Chem. Res.* **2000**, *39*, 2692.
23. Bouma,R. H. B.; Checchetti, A. *J. Memb. Sci.* **1997**, *128*, 141.
24. Car, A.; Stropnik, C.; Peinemann, K.-V. *Desalination* **2006**, *200*, 424.
25. Jun Hu, H. C.; Huiqing Ren, Yongming Wei, Zhengliang Xu, Honglai Liu and Ying Hu, *Ind. Eng. Chem. Res.* **2010**, *49*, 12605.
26. US Pat., 7637983, **2006**.
27. Song, Q. L.; Nataraj, S. K.; Roussenova, M. V.; Tan, J. C.; Hughes, D. J.; Li, W.; Bourgoin, P.; Alam, M. A.; Cheetham, A. K.; Al-Muhtaseb, S. A.; Sivaniah, E. *Energy Environ. Sci.* **2012**, *5*, 8359.
28. Nan, J.; Dong, X.; Wang, W.; Jin, W.; Xu, N. *Langmuir* **2011**, *27*, 4309.
29. Tae-Hyun Bae, J. S. L. *Indust. Eng. Chem. Res.* **2010**, *49*, 9863.
30. Hashemifard, S. A.; Ismail, A. F.; Matsuura, T. *J. Coll. Interf. Sci.* **2011**, *359*, 359.